IOP Publishing Plasma Physics and Controlled Fusion

Plasma Phys. Control. Fusion **58** (2016) 034011 (8pp) doi:10.1088/0741-3335/58/3/034011

Laser wakefield and direct acceleration with ionization injection

Xi Zhang[1], Vladimir N Khudik[1], Alexander Pukhov[2] and Gennady Shvets[1]

[1] Department of Physics and Institute for Fusion Studies, The University of Texas at Austin, Austin, TX 78712, USA
[2] Institut für Theoretische Physik I, Universität Düsseldorf, Düsseldorf 40225, Germany

E-mail: gena@physics.utexas.edu

Received 30 September 2015, revised 4 December 2015
Accepted for publication 22 December 2015
Published 9 February 2016

Abstract

We demonstrate using particle-in-cell simulations that electrons can be injected into a hybrid laser wakefield and direct laser accelerator via ionization injection. We propose an accelerator and injector scenario that utilizes two laser pulses. The first (pump) pulse produces the plasma 'bubble' by expelling the plasma electrons generated by its leading edge from the low-Z component of the gas mixture, and then injects electrons into the bubble by ionizing the high-Z component. The second time-delayed laser pulse resonantly interacts with these injected electrons undergoing betatron oscillations inside the bubble. We show that the electrons ionized off-axis and on-axis but off the peak ionization phase possess sufficient transverse energy to undergo efficient direct laser acceleration (DLA). When combined with their acceleration by the bubble's longitudinal plasma wake, DLA can double the total energy gain and produce a monoenergetic beam.

Keywords: ionization injection, laser wakefield acceleration, direct laser acceleration, plasma bubble regime

(Some figures may appear in colour only in the online journal)

1. Introduction

The development of laser-plasma accelerators [1] has been driven by the combination of the rapid advances in laser technology and the introduction of novel ideas that enabled higher quality, higher energy electron beams [2–4]. An example of one such idea in the area of laser-wakefield acceleration (LWFA) is the full plasma electron blow-out regime [5, 6], where an ultra-short laser pulse creates a relativistically moving plasma 'bubble' capable of trapping and accelerating plasma electrons to ultra-high energies. GeV-scale mono-energetic electron beams have been recently obtained [7–10] in the bubble regime. As LWFA matures, new acceleration mechanisms are being explored to further increase the electron energy gain and to broaden the scope of applications beyond high-energy physics, e.g. to novel compact radiation sources.

One such acceleration mechanism, proposed almost two decades ago [11, 12] but currently experiencing considerable renewed interest in the context of the electron acceleration in the bubble regime [13–20], is the direct laser acceleration (DLA). Unlike LWFA, DLA is a plasma-based acceleration mechanism that relies on the transverse component of laser's electromagnetic field to accelerate electrons. Resonant electron acceleration by the laser field takes place when the Doppler-shifted laser frequency $\langle\omega_d\rangle \equiv \omega_L(1-\langle v_x\rangle/v_{ph})$ matches the lth harmonic of the electron's betatron frequency $\omega_\beta = \omega_p/\sqrt{2}\,\langle\gamma^{-1/2}\rangle$. Here $\langle v_x\rangle$ and $\langle\gamma^{-1/2}\rangle$ are the time-averaged over a betatron period longitudinal velocity and inverse square root relativistic factor of the accelerated electron, ω_L and v_{ph} are the frequency and phase velocity of the laser field, and $\omega_p = \sqrt{4\pi ne^2/m}$ is the electron plasma frequency, and $l = 1, 3, 5\ldots$ is an odd number that corresponds to higher-order resonance for $l > 1$ [21, 22].

A key requirement for effective DLA is that the initial energy $\epsilon_\perp$ of betatron motion of an injected plasma electron be sufficiently high to overcome its rapid reduction due to electron acceleration by the longitudinal field of the plasma bubble [20].

Therefore, it is important to devise an appropriate injection scheme that satisfies this requirement. In general, electron injection in all plasma-based electron accelerators can be classified into density-based and laser-based. Density-based approaches involve shaping the longitudinal plasma density profile at the entrance of the as a single or multiple density ramps [20, 23–27]. A bump-shaped density profile has been suggested as a possible approach to injecting into a hybrid laser wakefield/direct laser accelerator [20].

Laser-based injection mechanisms do not require any plasma density engineering, and are generally considered to be experimentally simpler. Those include ionization of a high-Z gas [28–30], colliding multiple laser pulses [31, 32], and engineering rapid laser pulse evolution to produce a time-varying plasma bubble [9, 33–36]. Ionization injection is considered particularly straightforward because of its relative controllable and stable features. It has been demonstrated in multiple experiments [29, 37–39], and was theoretically shown to be promising for producing low-emittance beams [40, 41]. Note also that particle injection into the bubble due to the plasma field was experimentally verified in [38]. Here, we demonstrate that ionization injection is also an excellent injection mechanism into a laser wakefield and direct accelerator (LWDA), thus making it an attractive alternative to the earlier proposed [20] density-based injection into a LWDA.

The remainder of the paper is organized as follows. In section 2 we review the basic requirements for efficient LWDA and illustrate them by carrying out test particle simulation. The results of self-consistent 2D particle-in-cell (PIC) simulations carried out using the VLPL code are presented in section 3. We then classify several representative electrons that are injected via laser ionization and experience the combined laser wakefield and direct laser acceleration. Conclusions and the directions for future research are outlined in section 5.

2. Single-particle simulations

The theoretically proposed concept of the combined LWFA and DLA of electrons inside a plasma bubble, referred to below as a LWDA, enables synergistic combination of the two acceleration mechanisms [20]: their separate energy gains combine while the wakefield acceleration is further increased by delayed dephasing which is caused by large-amplitude betatron motion of the DLA electrons. However, a LWDA relies on two conditions: (a) spatio-temporal overlap between injected electrons and the laser field, and (b) large initial transverse energy $\epsilon_\perp = p_\perp^2/2\gamma m_e + m_e\omega_p^2 z^2/4$ [16, 20, 42]. The first condition is rather intuitive; it can be satisfied by using the double-peaked laser pulse format schematically shown in figure 2. Delaying the second (DLA) with respect to the bubble-forming (pump) pulse ensures that the injected electrons overlap with the DLA pulse as soon as they reach the rear portion of the bubble.

The second requirement examined in [20] is less intuitive; we illustrate it in this section by describing the results of single-particle simulations that track an ensemble of electrons moving in the prescribed electromagnetic fields of the laser and bubble. For simplicity, we assume planar linearly polarized laser fields in the form of $E_z^{(L)} = -E_0 \sin\omega_L(t - x/v_{ph})$ and $B_y^{(L)} = B_0 \sin\omega_L(t - x/v_{ph})$, where $B_0 = cE_0/v_{ph}$. The accelerating force and focusing forces inside the bubble produced by the combination of electric and magnetic fields are assumed in the form $W_x = m\omega_p^2(x - r_b - v_b t)/2e$ and $W_z = m\omega_p^2 z/2e$, respectively [42], where r_b and $v_b \simeq c(1 - 1/2\gamma_b^2)$ are the bubble's radius and group velocity.

The resulting equations of motion are given by [13, 17, 18, 20]

$$\begin{aligned}\frac{dp_x}{dt} &= -e\left(W_x - \frac{v_z}{c}B_y^{(L)}\right)\\ \frac{dp_z}{dt} &= -e\left(W_z + E_z^{(L)} + \frac{v_x}{c}B_y^{(L)}\right),\end{aligned} \tag{1}$$

where the specific simulation parameters listed in the caption of figure 1 were chosen to be consistent with PIC simulations presented in section 3. In the DLA mechanism, the laser electric field $E_z^{(L)}$ directly pumps energy into the transverse direction and the Lorentz force $\vec{v} \times \vec{B}^{(L)}/c$ from the laser magnetic field re-distributes the energy to the longitudinal direction. Initially (at $t = x = 0$) electrons are placed near the tail of the bubble and assigned a constant longitudinal momentum $p_x = \gamma_b mc$ to ensure their co-propagation with the bubble. The transverse initial conditions (z_0, p_{z0}) are chosen randomly inside the $0 < \epsilon_\perp \leqslant 2.3 m_e c^2$ phase space ellipse as shown in figure 1(a). Note that the assumption of an infinitely long laser pulse in the model above implies that the accelerated electrons overlap with the laser field at all times. As more realistic PIC simulations presented in section 3 indicate the electrons slip ahead of the DLA pulse, which also undergoes energy depletion.

The color-coded electron energy gain A_L from the laser plotted in figure 1(a) as a function of the initial conditions demonstrates that a large value of $\epsilon_\perp(t = 0)$ is a pre-condition for DLA [20]: only those electrons with large initial transverse energy gain considerable energy directly from laser. Qualitatively, this can be understood by noting that $dA_L/dt \propto \vec{E}_L \cdot \vec{p}_\perp/\gamma$, where A_L is the energy gained directly from the laser field. Therefore, the acceleration rate due to DLA is small if the initial $|\vec{p}_\perp|$ is small. The comparison of the A_L's of two representative DLA (red) and non-DLA (blue) electrons with the corresponding initial transverse energies $\epsilon_\perp^{DLA} = 1.8 m_e c^2$ and $\epsilon_\perp^{n-DLA} = 0.2 m_e c^2$ is shown in figure 1(b). While the DLA electron gains $A_L \approx 1100 m_e c^2$ from the laser, the non-DLA electron does not gain any appreciable energy.

The monotonic growth of A_L for the DLA electron shown in figure 1(b) indicates that the resonance is maintained between the laser field and the electron's betatron motion. To verify this conjecture, we plot the $\langle\omega_d\rangle$ and ω_β in figures 1(c) and (d) for the DLA and non-DLA electrons, respectively. Clearly, the resonance condition $\langle\omega_d\rangle \approx \omega_\beta$ is preserved for the DLA electron, but is quickly violated for the non-DLA electron. Note that no averaging is needed for the γ^{-1} in the expression for ω_β. The reason for this is that both electrons, however, gain considerable energy A_W directly from the wake: $A_W^{DLA} \approx 1200 mc^2$

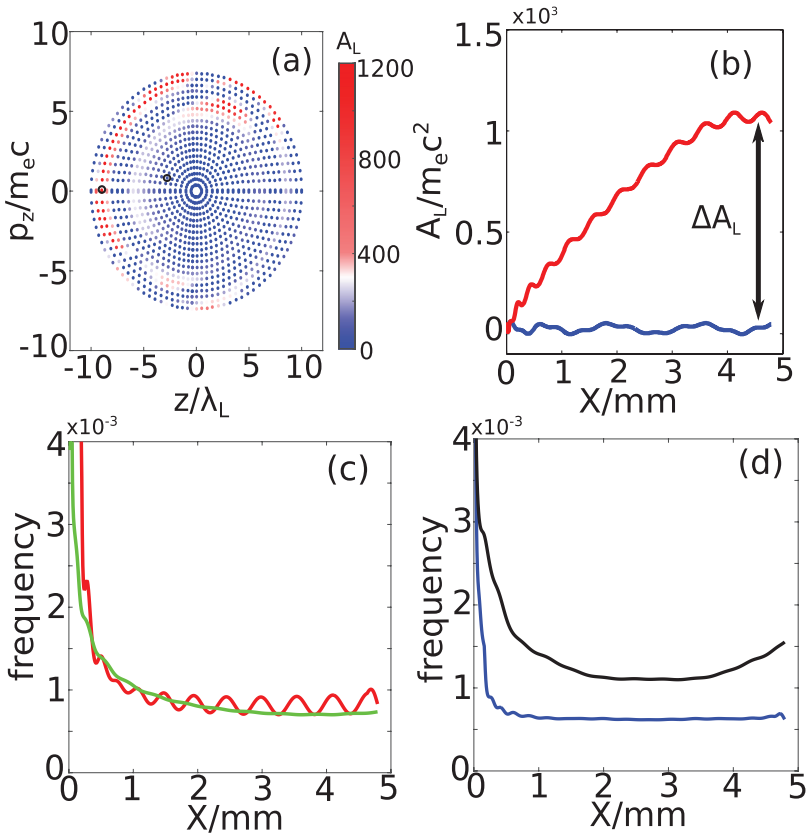

Figure 1. Single-particle dynamics in the combined wake and laser fields given by equation (1). (a) Color-coded energy gain A_L from the laser plotted as a function of the initial conditions. Elliptical curves: $\epsilon_\perp = \text{const}$ ($\max z = 10\lambda$ and $\max p_z = 7.4 m_e c$). (b) A_L for two representative electrons with initial conditions marked in (a) by circles. Red (blue) line: DLA (non-DLA) electrons. (c) Averaged Doppler-shifted laser frequency $\langle\omega_d\rangle$ (red line) and betatron frequency ω_β (green line) for the DLA electron from (b). (d)$\langle\omega_d\rangle$ (blue line), ω_β (black line) for the non-DLA electron from (b). Simulation parameters for equation (1): $E_0 \approx 2.3 m_e c\omega_L/e$, $r_b \simeq 15\lambda$, $\gamma_b = 12$, $v_{ph} = 1.0006c$, and $\omega_p/\omega_L = 0.048$.

and $A_W^{DLA} \approx 800mc^2$ at $x = 4$ mm. This steady energy gain washes out the high-frequency fluctuations in γ due to DLA.

To interpret the results presented in figures 1(c) and (d), it is instructive to examine the ultra-relativistic limits of $\langle\omega_d\rangle$ and ω_β:

$$\langle\omega_d\rangle \simeq \omega_L\left(\frac{1+\langle p_z^2\rangle/m_e^2c^2}{2\gamma^2}+\frac{1}{2\gamma_{ph}^2}\right), \quad \omega_\beta \simeq \frac{\omega_p}{\sqrt{2\gamma}}, \quad (2)$$

where we have introduced $\gamma_{ph} \equiv 1/\sqrt{v_{ph}^2 - 1}$. According to equation (2), the dependence of $\langle\omega_d\rangle$ on γ is much stronger that that of ω_β provided that γ_{ph} is very large. Therefore, the $\langle\omega_d\rangle < \omega_\beta$ condition is rapidly reached for the non-DLA electron as the electron's γ rapidly increases due to wakefield acceleration. The situation is drastically different for the DLA electron because of the rapid increase of p_z due to the laser field. Therefore, $\langle\omega_d\rangle$ decreases much slower for the DLA electron as compared with the non-DLA one, and the resonance condition is approximately preserved over the most part of the propagation distance. Due to the detuning between $\langle\omega_d\rangle$ and ω_β as shown in figure 1(c), the energy gain directly from the laser field of DLA electron saturates at the later times as shown in figure 1(d). After establishing the importance of large initial transverse energy for effective direct laser acceleration, we now proceed to demonstrating that this condition can be fulfilled using ionization injection into a bubble.

3. Particle-in-cell simulations of ionization injection in a LWDA

In this section, we use first-principles self-consistent relativistic 2D PIC code VLPL [43] to simulate ionization injection and acceleration of electrons to GeV energies in a LWDA. The schematic of a proposed LWDA is shown in figure 2 (see caption for simulations parameters). Multi-terawatt ($P_{pump} = 96$ TW and $P_{DLA} = 28$ TW) pump and the time-delayed DLA pulses are assumed in the simulation. Instead of engineering a density bump [20] for injecting electrons with large transverse energy, the injection due to the ionization of high-Z oxygen ions ($O^{7+} \rightarrow O^{8+}$) is modeled in the simulation. The 100 μm-long gas mixture region consisting of 90% H_e and 10% O_2 is shown as a dark area in figure 2.

The leading edge of the pump pulse fully ionizes helium and the low-charge states of oxygen ions, thereby creating a background plasma with the density $n_0 = 4.0 \times 10^{18}$ cm^{-3} which is pushed aside by the pump pulse to create a plasma bubble. The K-shell oxygen's electrons are produced via ionization close to the peak of the pump pulse intensity.

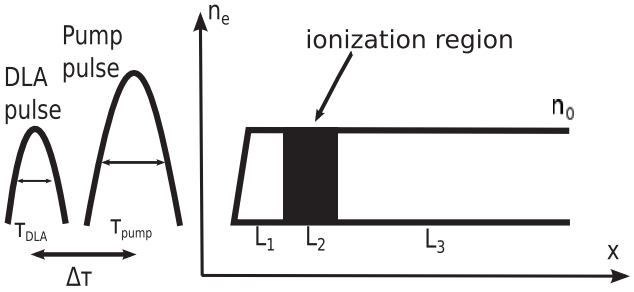

Figure 2. Schematic representation of the laser pulse format and plasma density profile. Plasma parameters: $L_1 = 80\ \mu$m, mixed gas length $L_2 = 100\ \mu$m, $L_3 \simeq 3$ mm; $n_0 = 4.0 \times 10^{18}$cm^{-3}, $n_{O^{7+}} = 0.1 n_0$, ionization potential for $O^{7+} \rightarrow O^{8+}$ $U_{\rm ion} \simeq 871.4$ ev, $\lambda_p = 2\pi c/\omega_p = 17\ \mu$m. Laser parameters: wavelength $\lambda_{\rm L} = 0.8\ \mu$m, $I_{\rm pump} = 2.3 \times 10^{19}$ W cm^2, $I_{\rm DLA} = I_{\rm pump}/2$, pulse durations $\tau_{\rm pump} = 20$ fs and $\tau_{\rm DLA} = 15$ fs, spot size $w_{\rm pump} = 17\ \mu$m and $w_{\rm DLA} = 13\ \mu$m, inter-pulse time delay $\Delta\tau = 61$ fs. Simulation parameters: numerical grid cell size $\Delta x \times \Delta z = \lambda_{\rm L}/50 \times \lambda_p/70$, four macroparticles per cell.

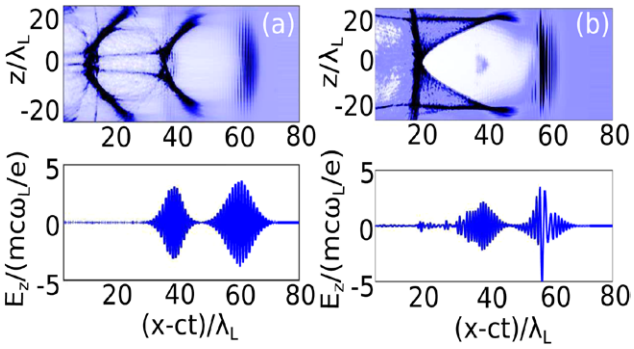

Figure 3. (a) Plasma electron density (top) and the on-axis laser field E_z at $x = 320\ \mu$m. (b) Same as (a), but at $x = 2.6$ mm.

Therefore, these electrons are injected and get trapped inside the plasma bubble [29, 37–39]. The pump pulse thus serves a dual role of producing the plasma bubble and injecting the electrons into it.

The results of the PIC simulations are presented in figures 3(a) and (b) for $x = 320\ \mu$m (right after the lasers passing though the ionization region) and $x = 2.6$ mm (peak energy gain), respectively. The ADK tunneling ionization model [44–46] is used to describe the release of the K-shell electrons from the oxygen ion. It is apparent from the top panel of figure 3(a) that the majority of trapped electrons are concentrated at the bottom of plasma bubble where the DLA pulse is located. The plasma bubble also serves as a guiding structure for the DLA pulse. As the laser pulses and the plasma bubble propagates through the plasma, the injected electrons advanced forward through the bubble due to dephasing according to [20]:

$$\frac{{\rm d}\zeta}{{\rm d}(ct)} \approx \frac{1}{2\gamma_b^2} - \frac{1 + \langle p_z^2/m_e^2c^2\rangle}{2\gamma^2}, \qquad (3)$$

where $\zeta = x - v_b t$. Even after the electrons reach the middle of the bubble as shown in figure 3(b), their overlap with the DLA pulse is well maintained. The reason is that the DLA pulse, which propagates inside the plasma bubble, has a highly relativistic group velocity ($\gamma_{DLA} \simeq 40$) that is larger than the

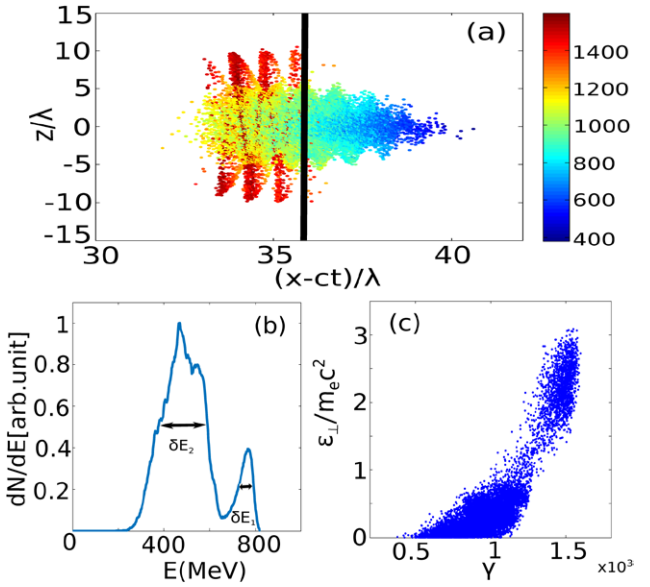

Figure 4. (a) Spatial distribution of the ionization injected electrons color-coded according to their relativistic factor γ at $x = 2.6$ mm; black vertical line: bubble's center. (b) Energy spectrum for injected elelctrons. Energy spreads: $\delta E_1 \simeq 60$ MeV, $\delta E_2 \simeq 230$ MeV. (c) Bifurcated phase space (γ, $\epsilon_\perp$) shows positive correlation between total and transverse energies for DLA electrons.

bubble group velocity ($\gamma_b \sim 15$) and very close to the longitudinal velocity of the DLA electrons. The expansion of the plasma bubble [33, 34] observed by comparing the top panels of figures 3(a) and (b) also plays a role in maintaining excellent overlap between the DLA pulse and the injected electrons near the middle of the plasma bubble.

Close observation of figure 3(b) and its zoomed-in version in figure 4(a) shows that DLA and non-DLA particles are spatially separated in x. This is the consequence of equation (3) which predicts that DLA electrons with large betatron amplitudes advance less through the bubble than the non-DLA electrons. The resulting phase space bifurcation in the LWDA is apparent from figure 4(a), where the injected electrons are color-coded according their total energy γmc^2, and the vertical black line indicates the center of plasma bubble($E_x \simeq 0$). The high-energy DLA group of electrons is located behind the lower-energy non-DLA group, which is already in the decelerating region of the bubble.

The total energy spectrum of the accelerated electrons are plotted in figure 4(b). The spectrum has two peaks which represent the DLA ($\gamma^{\rm DLA}mc^2 \approx 770$ MeV) and non-DLA electrons ($\gamma^{\rm n-DLA}mc^2 \approx 450$ MeV), respectively. The DLA effect does not compromise the beam's energy spread; in fact, the energy distribution of the DLA electrons is considerably lower than that of the non-DLA electrons.

Below we present a quantative statistics of the ionized electrons. The number of trapped electrons is about 90% of all electrons released by oxygen ionization. There are about 13% of electrons undergoing significant DLA within the group of trapped electrons or about 11% within the group of all electrons released by ionization. DLA electrons form a subpopulation of high transverse energy electrons, that were born either off-axis or off-peak phase. The ADK ionization rate is

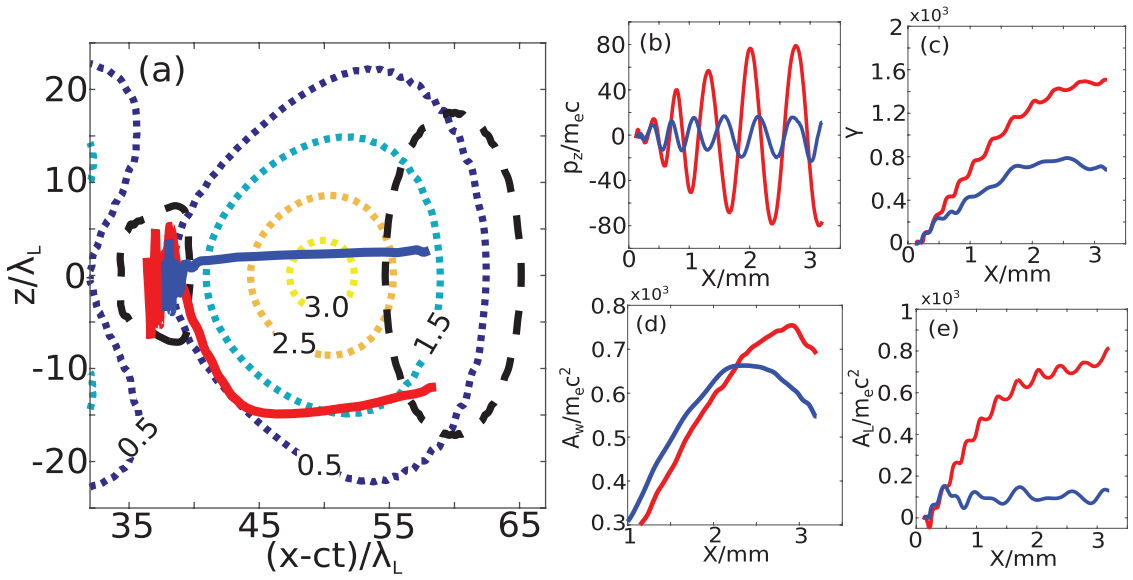

Figure 5. The evolution of ionization-injected electrons in the plasma bubble. (a) Trajectories of the representative DLA (red solid curve) and non-DLA (blue solid curve) electrons. Colored dotted curves: the labelled $e\Psi/m_ec^2 = \text{const}$ contours of the wake's potential. Black dashed curves: $E_z/E_z^{\max} = 0.45$ contour inside which 99% of ionization events takes place. (b)–(e) The long-term evolution of the transverse momentum p_z, relativistic factor γ, the work A_w done by the wake, and work A_L done by the laser for the same representative electrons as in (a). Simulation parameters: same as in figure 2.

relatively small when it is off-axis or off-peak phase. So the number of DLA electrons is smaller than the number of non-DLA electrons.

Due to the 2D geometry, we can only roughly estimate the charge yield. The beam density is $n \sim 8 \times 10^{17}$ cm^{-3}at the propagation distance $x = 2.6$ mm as shown in figure 4. The length of the beam is about $L_b \sim 6$ μm and the radius is about $r_b \sim 4$ μm. We estimate that there is about $40pC$ charge in the beam.

Another intriguing difference between DLA and non-DLA electrons is revealed in figure 4(c) which shows the bifurcated $(\gamma, \epsilon_\perp)$ phase space of the accelerated electrons. The DLA group exhibits a clear positive correlation between γ and $\epsilon_\perp$ while there is no such correlation for the non-DLA group. Both the double-peaked energy spectrum and the birurcated phase space are reminiscent of the earlier results [20] obtained using the density bump injection. However, the key finding of the present work is that the synergistic LWFA and DLA mechanisms can be realized in an accelerator with ionization injection. In the next section we examine the mechanisms responsible for providing large initial transverse energies to the electrons produced using tunneling ionization.

4. Mechanisms of ionization injection

To understand how laser-ionized electrons can acquire large transverse energy necessary for DLA, we need to recall the specifics of ionizing an atom in a laser field that greatly exceeds the atomic electric field $E_a = e/r_e^2 \simeq 5.1$ GV cm^{-1}, where $r_e = e^2/m_ec^2$ is the classical electron radius. According to the ADK tunneling ionization model [44–46], the ionization rate is given by the following expression:

$$W(t) = \omega_a C \left(\frac{E_{\text{ion}}}{E_{\text{L}}(t)}\right)^d \exp\left[-\frac{E_{\text{ion}}}{E_{\text{L}}(t)}\right], \tag{4}$$

where $\omega_a = \alpha^2 c/r_e$ is the atomic frequency unit, $\alpha = 1/137$ is the fine structure constant, and for the $O^{7+} \to O^{8+}$ oxygen ionization we estimate that $C \approx 8.4 \times 10^4$, $d \approx 1$ and $E_{\text{ion}} \approx 1.7 \times 10^3$ GV cm^{-1}. ADK tunneling ionization model implemented in VLPL [45, 46] assumes that the ionization rate is given by equation (4).

From equation (4) we conclude that for the peak on-axis electric field of the laser $E_0 = 3.5mc\omega_L/e$ and the pulse duration of $\tau_{\text{pump}} = 20$ fs, the product $W(E_0)\tau_{\text{pump}} \gg 1$. This means that an O^{7+} ion located on the laser axis is ionized to its O^{8+} state with nearly 100% probability. This also implies that an atom experiencing a weaker instantaneous field $E_L(t) < E_0$ can also lose an electron with significant probability. In the near-static tunneling limit of $\omega_L \ll \omega_a$ electron tunneling may occur according to the following scenarios: (a) at $z \neq 0$ (off-axis tunneling), or (b) at $z = 0$, but at the electric field's phase ϕ that does not correspond to it's maximum (off-peak phase ionization). Of course, all intermediate scenarios are also possible, so the (a) and (b) are the two limiting cases that supply ionization-produced electrons with finite transverse energy $\epsilon_\perp$ necessary for DLA acceleration. The scenarios (a) and (b) are illustrated by figures 5(a) and 6(a) respectively.

The motion of an ionized electron born at rest inside the pump pulse can be broken up into three stages: (i) ionization and direct interaction with the pump laser pulse, (ii) initial trapping in the bubble, and (iii) final acceleration by the combination of LWFA and DLA mechanisms. The first two stages are very short and result in the electron's energy gain of the order of $\gamma_b m_e c^2$. The third stage is the longest one; it results

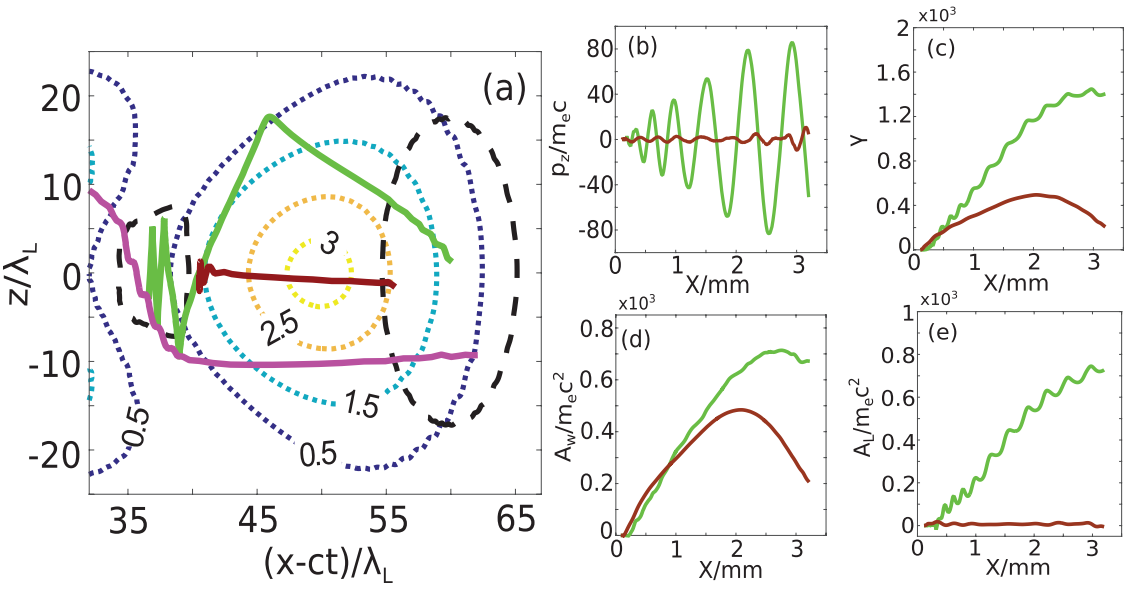

Figure 6. Same as in figure 5, but for a different set of ionization-injected electrons: the untrapped (magenta line), the deeply trapped non-DLA (brown line), and the ricochet DLA (green line) electrons. (b)–(e): same as in figure 5, but for the deeply trapped non-DLA and the DLA ricochet electrons.

in the final energy gain exceeding $2\gamma_b^2 m_e c^2$. Because the third stage of the electron acceleration in an LWDA was previously analyzed in some detail [20], below we concentrate mostly on the first and second acceleration stages, as well as on the earliest times of the third stage.

During the *first stage* of the duration $\Delta\tau_1 \sim \tau_{\rm pump}$ the electron born at $t = t_i$ at $(x = x_i, z = z_i)$ interacts primarily with the pump pulse. This interaction is best described using the (approximate) conservation of the transverse canonical momentum: $p_z(t)/m_e c - a_z(z(t), t) = p_z(t_i)/m_e c - a_z(z_i, t_i)$, where $a_z = eA_z/m_e c^2$ is the normalized canonical momentum of the laser. This approximation is valid as long as the laser spot size satisfies $w_{\rm pump} \gg z_{\rm wiggle}$, where $z_{\rm wiggle}$ is the wiggling amplitude of the newly-ionized electron in the laser field. Combining the $a_z(t) = 0$ for $t > t_i + \tau_{\rm pump}$ condition with $p_z(t_i) = 0$, we obtain $p_{z0}/m_e c = -a_z(z_i, t_i)$ at the end of the first stage.

Assuming that $A_z = cg(z)E_0 \cos\omega_{\rm L}(t - x/v_{\rm ph})/\omega_{\rm L}$, where $g(z)$ is the transverse laser profile normalized as $g(z = 0) = 1$, we obtain [40, 41]

$$p_{z0} = -g(z_i)\frac{eE_0}{mc\omega_{\rm L}}\cos\phi_i, \tag{5}$$

where $\phi_i = \omega_{\rm L}(t_i - x_i/v_{\rm ph})$ is the laser phase at the moment of electron's tunneling from an oxygen ion in the electric field of the magnitude $|E_i| = E_0 g(z_i)|\sin\phi_i|$. By definition, the peak-phase ionization corresponds to $\phi_i = \pm\pi/2$ and vanishing transverse momentum p_{z0} while the off-peak ionization corresponds to $\phi_i \neq \pm\pi/2$ and $p_{z0} \neq 0$. Therefore, those electrons born far off-axis are likely to be produced by peak-phase ionization and to have small p_{z0}. On the other hand, the on-axis electrons can be ionized during the off-peak phase of the laser and have a relativistic $p_{z0} \sim eE_0/mc\omega_{\rm L}$. However, both off-axis and off-peak electrons can have a substantial initial transverse energy $\epsilon_{0\perp} = p_{z0}^2/2\gamma_0 m_e + m_e\omega_p^2 z_0^2/4$ (where $z_0 = z_i$) that is necessary for effective DLA.

The second stage involves electron's motion toward the back of the bubble and its subsequent trapping. Because of the brevity of the first stage, we assume that the electron's initial conditions established for the second stage are $(z_0, p_{z0}, x_i, p_{x0} = 0)$. Assuming that the bubble does not have sufficient time to evolve during the second stage, we can take advantage of the conservation of the moving frame Hamiltonian (MFH) [29, 34, 42] given by

$$H = \gamma m_e c^2 - v_b p_x - e\Psi \tag{6}$$

where $\Psi = \frac{v_b}{c}A_x - \Phi$ is the wake potential constructed from its vector potential and scalar potentials A_x and Φ, respectively. Using the results of the PIC simulations, we can approximately calculate $\Psi(\zeta, z)$ at any instance of time according to $\Psi = \int_{\zeta_{\rm min}}^{\zeta_{\rm max}} E_x {\rm d}\zeta$, where E_x is the longitudinal electric field, and the integration is carried out over the entire moving computational window that encompasses the plasma bubble. The contours of constant $e\Psi(\zeta, z)/m_e c^2$ calculated at $x = 120$ μm inside the ionization region shown in figure 2 are presented in figures 5(a) and 6(a). For this particular case we have found that the maximum value of Ψ at the center of the bubble is $\Psi_{\rm max} \approx 3.1 m_e c^2/e$ while its minimum value at the bottom of the bubble is $\Psi_{\rm min} \approx 0.1 m_e c^2/e$.

It is instructive to simplify the expression for the MFH in the two important limits: at the end of the first acceleration stage, when $p_x/m_e c \ll \gamma_0 \sim 1$, and at the end of the second stage, when $\gamma_b \leqslant \gamma_0 \ll \gamma_b^2$. In the former case we can assume that $H_0 \approx \gamma_0 m_e c^2 - e\Psi(\zeta_i, z_i)$ while in the latter case $H_f \approx -e\Psi(\zeta_t, z_t)$, where $(\zeta_{i,t}, z_{i,t})$ are the coordinates of electrons birth/trapping inside the plasma bubble. From $H_0 = H_f$ we derive the following trapping condition for the electrons:

$$\frac{e(\Psi_i - \Psi_f)}{m_e c^2} \approx \gamma_0 \sim 1, \tag{7}$$

where $\Psi_i \equiv \Psi(\zeta_i, z_i)$ and $\Psi_f \equiv \Psi(\zeta_f, z_f)$.

The constant-Ψ contours can be used for a simple graphical interpretation of the trapping condition given by equation (7). If an electron is born on the Ψ_i contour, then it will slip out of the bubble if $\Psi_i < \Psi_{\min} + \gamma_0 m_e c^2/e$. This condition is exemplified by a representative magenta-colored electron shown in figure 6(a) born at the leading edge of the pump. This electron, which starts insufficiently deep inside the bubble with $\Psi_i \approx 0.5 m_e c^2/e$, does not get trapped inside the bubble. On the other hand, all other representative electrons shown in figures 5 and 6 that are born deep inside the bubble ($\Psi_i > 1.2 m_e c^2/e$) end up trapped inside the bubble because the trapping condition $\Psi_i > \Psi_{\min} + \gamma_0 m_e c^2/e$ is satisfied for them.

Now we consider the *third acceleration stage* involving the long-term interaction of the trapped electrons with the DLA pulse and with the bubble's wakefield. The trajectories of two typical trapped electrons are shown in figure 5(a) over a distance of $x < 0.8$ mm after their ionization. The electrons are chosen to belong to the DLA (red) and non-DLA (blue) groups. The pump laser's intensity contour shown with a dashed line was chosen in such a way that 99% of all ionization events take place inside the contour based on ADK the tunneling ionization model [44, 45]. We observe that the non-DLA electron is born near the axis and during the peak ionization phase $\phi_i \approx \pi/2$. Therefore, this electron does not acquire any significant initial transverse energy $\epsilon_{0\perp}$ during the first acceleration stage. Even though the non-DLA electron spatially overlaps with the DLA laser pulse as illustrated in figure 5(a), its interaction with the laser is weak because its initial transverse energy is small. On the other hand, the DLA electron is produced via off-axis peak-phase ionization at $z_i \approx 11\lambda_L$ with considerable $\epsilon_{0\perp}$.

The long-time acceleration of these two representative electrons shown confirms their classification as DLA and non-DLA. The energy gains $A_w = -\int eE_x v_x \mathrm{d}t$ and $A_L = -\int eE_z v_z \mathrm{d}t$ from the wake are plotted in figures 5(d) and (e), respectively. The DLA electron gains much more energy ($\Delta A_L \approx 700 m_e c^2$) directly from the laser than non-DLA electron. Meanwhile, the DLA electron also gains more energy ($\Delta A_W \approx 100 m_e c^2$) from the wake than a non-DLA electron because of the delayed dephasing predicted by equation (3). The delayed dephasing of the DLA electron with respect to the non-DLA one is observed by comparing the peaks of the two $A_W(x)$ curves in figure 5(d). The non-DLA electrons lose about 50–100 MeV due to the dephasing. The combination of these two factors provide the DLA electron with much larger higher peak energy $\gamma m_e c^2$ as shown in figure 5(c).

Two more electron injection and acceleration scenarios are illustrated in figure 6, where the trajectories of a non-DLA (brown-colored) and DLA (green-colored) trapped electrons are shown in figure 6(a). The non-DLA electron is born near the trailing edge of the pump pulse deep inside the bubble at $\Psi_i \approx 2.5 m_e c^2/e$. The conservation of the MFH expressed by equation (7) implies that the electron does not reach the back of the bubble and, therefore, does not overlap with the DLA pulse. The direct laser energy gain A_L is, therefore, negligible, i.e. even smaller than for the non-DLA electron analyzed in figure 5.

The DLA electron shown in figure 6 exemplify the electrons injected via the off-peak phase tunneling [47]. Even though the electron is produced by laser ionization on-axis, its trajectory shown in figure 6(a) clearly indicates that it has a large transverse momentum after the first acceleration stage. The initial transverse momentum of the electron is estimated to be $P_{0z} \approx 2.2 m_e c$. Because of its unusual trajectory that involves several bounces off the edge of the plasma bubble before overlapping with the DLA pulse and undergoing further acceleration, we refer to such particles as 'ricochet' electrons. By following the long-term acceleration of the ricochet DLA electron shown in figures 6(b)–(e), we conclude that the efficiency of DLA is comparable for the electrons produced via off-axis and off-peak tunneling. Therefore, we conclude that the DLA electrons injected into the bubble via ionization injection roughly belong to two categories: the off-axis ionized and the off-peak phase ionized (ricochet) electrons.

5. Conclusion

In conclusion, we have demonstrated that ionization injection is suitable for a laser wakefield and direct accelerator (LWDA) that relies on the hybrid laser wakefield and direct laser acceleration mechanism for achieving the highest energy gain. We find that the electrons' energy spectrum is split into two peaks corresponding to two sub-populations: the higher-energy DLA and the lower-energy non-DLA particles. By tracking several electrons with different initial condition, we demonstrate that DLA electrons born inside the plasma bubble must have significant transverse energy. Two ways of gaining such energy are discovered using PIC simulations: electrons must be generated either via off-axis of via off-peak phase tunneling. With the introduction of ionization injection, the hybrid laser wakefield and direct laser plasma accelerator may potentially become more stable and controllable. High energy DLA electrons generated in LWDA may have future applications as the sources of x-rays.

Acknowledgments

This work was supported by DOE grants DE-SC0007889 and DE-SC0010622, and by an AFOSR grant FA9550-14-1-0045. The authors thank the Texas Advanced Computing Center for providing HPC resources.

References

[1] Tajima T and Dawson J 1979 *Phys. Rev. Lett.* **43** 267
[2] Faure J, Glinec Y, Pukhov A, Kiselev S, Gordienko S, Lefebvre E, Rousseau J, Burgy F and Malka V 2004 *Nature* **431** 54
[3] Geddes C, Toth C, Van Tilborg J, Esarey E, Schroeder C, Bruhwiler D, Nieter C, Cary J and Leemans W 2004 *Nature* **431** 538
[4] Mangles S *et al* 2004 *Nature* **431** 535

[5] Pukhov A and Meyer-Ter-Vehn J 2002 *Appl. Phys.* B **74** 355–61
[6] Li Z, Tsai H-E, Zhang X, Pai C-H, Chang Y-Y, Zgadzaj R, Wang X, Khudik V, Shvets G and Downer M C 2014 *Phys. Rev. Lett.* **113** 085001
[7] Leemans W, Nagler B, Gonsalves A, Toth C, Nakamura K, Geddes C, Esarey E, Schroeder C and Hooker S 2006 *Nat. Phys.* **2** 696
[8] Leemans W *et al* 2014 *Phys. Rev. Lett.* **113** 245002
[9] Wang X *et al* 2013 *Nat. Commun.* **4** 1988
[10] Kim H T, Pae K H, Cha H J, Kim I J, Yu T J, Sung J H, Lee S K, Jeong T M and Lee J 2013 *Phys. Rev. Lett.* **111** 165002
[11] Pukhov A, Sheng Z-M and Meyer-ter-Vehn J 1999 *Phys. Plasmas* **6** 2847
[12] Gahn C, Tsakiris G D, Pukhov A, Meyer-ter-Vehn J, Pretzler G, Thirolf P, Habs D and Witte K J 1999 *Phys. Rev. Lett.* **83** 23
[13] Nemeth K, Shen B, Li Y, Shang H, Crowell R, Harkay K C and Cary J R 2007 *Phys. Rev. Lett.* **100** 095002
[14] Cipiccia S *et al* 2011 *Nat. Phys.* **7** 867
[15] Nam I, Hur M S, Uhm H S, Hafz N A M and Suk H 2011 *Phys. Plasmas* **18** 043107
[16] Corde S, Ta Phuoc K, Fitour R, Faure J, Tafzi A, Goddet J P, Malka V and Rousse A 2011 *Phys. Rev. Lett.* **107** 255003
[17] Ta Phuoc K, Esarey E, Leurent V, Cormier-Michel E, Geddes C G R, Schroeder C B, Rousse A and Leemans W P 2008 *Phys. Plasmas* **15** 063102
[18] Ta Phuoc K, Corde S, Fitour R, Shah R, Albert F, Rousseau J-P, Burgy F, Rousse A, Seredov V and Pukhov A 2008 *Phys. Plasmas* **15** 073106
[19] Shaw J L, Tsung F S, Vafaei-Najafabadi N, Marsh K A, Lemos N, Mori W B and Joshi C 2014 *Plasma Phys. Control. Fusion* **56** 084006
[20] Zhang X, Khudik V N and Shvets G 2015 *Phys. Rev. Lett.* **114** 184801
[21] Khudik V N, Zhang X and Shvets G 2015 Far-field constant-gradient laser accelerator of electrons in an ion channel, under review
[22] Khudik V N, Arefiev A V, Zhang X and Shvets G 2016 *Phys. Plasmas* submitted
[23] Suk H, Barov N and Rosenzweig J B 2001 *Phys. Rev. Lett.* **86** 1011
[24] Geddes C G R, Nakamura K, Plateau G R, Toth Cs, Cormier-Michel E, Esarey E, Schroeder C B, Cary J R and Leemans W P 2008 *Phys. Rev. Lett.* **100** 215004
[25] Schmid K, Buck A, Sears C M S, Mikhailova J M, Tautz R, Herrmann D, Geissler M, Krausz F and Veisz L 2010 *Phys. Rev. Spec. Top. Accel. Beams* **13** 091301
[26] Buck A *et al* 2013 *Phys. Rev. Lett.* **110** 185006
[27] Gonsalves A J *et al* 2011 *Nat. Phys.* **7** 862
[28] Chen M, Sheng Z-M, Ma Y-Y and Zhang J 2006 *J. Appl. Phys.* **99** 056109
[29] Pak A, Marsh K A, Martins S F, Lu W, Mori W B and Joshi C 2010 *Phys. Rev. Lett.* **104** 025003
[30] Chen M, Esarey E, Schroeder C B, Geddes C G R and Leemans W P 2012 *Phys. Plasmas* **19** 033101
[31] Esarey E, Hubbard R F, Leemans W P, Ting A and Sprangle P 1997 *Phys. Rev. Lett.* **79** 2682
[32] Lehe R, Lifschitz A F, Davoine X, Thaury C and Malka V 2013 *Phys. Rev. Lett.* **111** 085005
[33] Kalmykov S Y, Beck A, Yi S A, Khudik V N, Downer M C, Lefebvre E, Shadwick B A and Umstadter D P 2011 *Phys. Plasmas* **18** 056704
[34] Kalmykov S, Yi S A, Khudik V and Shvets G 2009 *Phys. Rev. Lett.* **103** 135004
[35] Yi S A, Khudik V, Kalmykov S Y and Shvets G 2011 *Plasma Phys. Control. Fusion* **53** 014012
[36] Yi S A, Khudik V, Siemon C and Shvets G 2013 *Phys. Plasmas* **20** 013108
[37] Liu J S *et al* 2011 *Phys. Rev. Lett.* **107** 035001
[38] Oz E *et al* 2007 *Phys. Rev. Lett.* **98** 084801
[39] McGuffey C *et al* 2010 *Phys. Rev. Lett.* **104** 025004
[40] Xu X L *et al* 2010 *Phys. Rev. Spec. Top. Accel. Beams* **17** 061301
[41] Schroeder C B, Vay J-L, Esarey E, Bulanov S S, Benedetti C, Yu L-L, Chen M, Geddes C G R and Leemans W P 2010 *Phys. Rev. Spec. Top. Accel. Beams* **17** 101301
[42] Kostyukov I, Pukhov A and Kiselev S 2004 *Phys. Plasmas* **11** 11
[43] Pukhov A 1999 *J. Plasma Phys.* **61** 425
[44] Ammosov M V, Delone N B and Krainov V P 1986 *Sov. Phys. JETP* **64** 1191
[45] Chen M, Cormier-Michel E, Geddes C G R, Bruhwiler D L, Yu L L, Esarey E, Schroeder C B and Leemans W P 2012 *J. Comput. Phys.* **236** 220
[46] Karmakar A and Pukhov A 2007 *Laser Part. Beams* **25** 371
[47] McNaught S J, Knauer J P and Meyerhofer D D 1997 *Phys. Rev. Lett.* **78** 626